Catalysis Science & Technology

ROYAL SOCIETY OF CHEMISTRY

PAPER

View Article Online
View Journal

Cite this: DOI: 10.1039/d5cy00306g

Role of long-chain carboxylate ligands in glycerol dehydrogenation catalyzed by Co decorated nanoparticles†

Chaima Hammed, [a] Xiaojing Wu,[b] Anis Gannouni,[a] Wahiba Najjar[a] and Carine Michel *[b]

Acceptorless dehydrogenation of alcohols is a green process to obtain several added-value products such aldehydes and ketones and H_2. Decorated Co nanoparticles have shown great catalytic activity in this reaction. In this catalytic system, long-chain carboxylate ligands are present to protect the Co nanoparticles from aggregation and oxidation and to stabilize their shape. The most active shape is as a nanorod, exposing mainly the Co(0001) and Co(11–20) surfaces. We propose here the combination of classical molecular dynamics and DFT to better understand the role of carboxylate ligands when decorated Co nanorods are used as catalysts in glycerol dehydrogenation. Classical molecular dynamics simulations provided the free energy of adsorption at the interface as a function of the ligand surface coverage on the two mainly exposed facets Co(0001) and Co(11–20). This allows us to determine the possible organization of carboxylate ligands around the active site using DFT to investigate the activity and selectivity of glycerol dehydrogenation into dihydroxyacetone (DHA) or glyceraldehyde (GLYA) on the two exposed facets. We found that DHA, which is the thermodynamic product, is predicted to be the dominant product. Pristine Co(11–20) and decorated Co(0001) are the most active surfaces, showing that the presence of ligands can alter the structure sensitivity of a reaction, an effect that needs to be taken into account in the design of shaped decorated metallic nanoparticles to be used as catalysts.

Received 12th March 2025,
Accepted 18th July 2025

DOI: 10.1039/d5cy00306g

rsc.li/catalysis

1. Introduction

The catalytic acceptorless dehydrogenation of alcohols (ADA) garners significant attention due to its ability to produce valuable carbonyl compounds and directly generate molecular hydrogen.[1] This process is highly attractive in terms of efficiency and safety, as it obviates the need for hydrogen acceptors like O_2, sacrificial carbonyl compounds, or alkenes, and prevents the formation of organic and inorganic waste by-products.[2] However, this reaction is thermodynamically unfavourable at room temperature. Nevertheless, the release of H_2 provides a positive entropic contribution, allowing the equilibrium to shift in a favourable direction through the removal of H_2.[3]

Glycerol ($C_3H_8O_3$) has been suggested as a possible source for H_2 production. It is derived from oils and fats through various processes, and it is also a by-product of biodiesel production.[4] It can be transformed into value-added chemicals such as dihydroxyacetone (DHA),[5–8] glyceraldehyde (GLYA),[9–11] propanediol,[12–14] lactic acid[15,16] and other products.[17] Among these value-added chemicals, DHA and GLYA are two of the most attractive products due to their high demand in the cosmetic and pharmaceutical industries.[18–20] They can be obtained by the ADA process, but then a mixture of these two products may be obtained since DHA results from the dehydrogenation of the secondary hydroxyl and GLYA from the dehydrogenation of one of the two primary hydroxyls of glycerol.

In 2010, Crotti *et al.*[21] shed light on the direct dehydrogenation of glycerol into DHA on catalyzed iridium (Ir) complexes with P–N ligands. They demonstrated that selective glycerol conversion into DHA and GLYA is achievable. After that, several experimental and theoretical studies on glycerol dehydrogenation *via* homogeneous[22,23] and heterogeneous[10,24–27] catalysts were carried out.[28] For example, Feng *et al.* utilized the dehydrogenation of glycerol to glyceraldehyde on Pt/C NPs to further produce 1,2-PDO with 37% conversion of glycerol.[9] Liu *et al.* studied a theoretical approach on Rh(111), Pt(111), Cu(111), Pd(111) and Ni(111) surfaces, mentioning better catalytic activity for glycerol dehydrogenation on Rh, Pd, and Ni and less on Cu.[29] Auneau *et al.* investigated glycerol hydrogenolysis on Rh,

[a] *Laboratory of Materials Chemistry and Catalysis LR01ES08, Faculty of Sciences of Tunis, University of Tunis El Manar, 2092, Tunis, Tunisia*
[b] *LCH, CNRS, ENS de Lyon, UMR 5182, 69342, Lyon Cedex 07, France.*
E-mail: carine.michel@ens-lyon.fr

† Electronic supplementary information (ESI) available. See DOI: https://doi.org/10.1039/d5cy00306g

combining DFT and experimental approaches. They found that the first step is the glycerol dehydrogenation into GLYA rather than DHA due to lower barriers to dehydrogenate the terminal position.[10]

Recently, we demonstrated that Co and Co alloys such as CoRu (ref. 30) and core–shell CoCu (ref. 31) exhibit favourable catalytic properties in the ADA reaction; in particular, unsupported Co nanorods display high chemo-selectivity across a broad range of substrates, encompassing linear and cyclic alcohols, and show excellent recyclability, maintaining their activity, selectivity, and anisotropic shape over three consecutive runs.[32–34] These Co nanorods are decorated with long-chain carboxylate ligands and majorly expose two types of surface facets, (0001) and (11–20) facets. Our DFT investigations on these two facets identified (11–20) as the most active facet. Besides, the chemo-selectivity was assessed on that facet, comparing the dehydrogenation pathways of propan-1-ol and propan-2-ol. The aldehyde is so strongly bonded that it would poison the surface rather than desorb, while the ketone can desorb easily, which is in favor of strong selectivity towards secondary alcohols. Still, this analysis did not include the possible effect of carboxylate ligands on the adsorption/desorption and on the reaction pathways.

Previous research has shown that the co-adsorption of species such as ligands,[35] other alcohols,[36] water[37,38] or hydrogen[39,40] could actually have an influence on the catalytic process of the dehydrogenation reaction of the alcohol. Pandey *et al.*[41] provided a mechanistic perspective on the ligand–metal role in the alcohol dehydrogenation reaction and found that it facilitates substrate activation and paves a low-energy dehydrogenation pathway. In 2020, Kaźmierczak *et al.* studied the importance of the decoration of cobalt NPs (Co(0001) and Co(11–20)) using acetate as a model ligand. The presence of acetate influenced the adsorption energies of intermediates through hydrogen bonding,[33] leading to a stronger catalytic activity on both facets. In this study, the ligands were located in their ideal positions. A catalytic cavity was arbitrarily created in a dense organized monolayer of acetate ligands. Understanding how the film may fluctuate is important, but exploring these effects requires moving to molecular mechanics to reach the next scale in term of time and size. This is now possible thanks to the recent development of a bespoke Co–O interfacial force field that was built to describe the interaction between carboxylate ligands and metallic Co surfaces.[42]

Benefiting from this recent development, we propose here a strategy based on the combination of classical molecular dynamics and DFT to investigate the role of the decoration of Co(0001) and Co(11–20) surfaces in the selectivity of the acceptorless dehydrogenation of glycerol into DHA and GLYA. We first determine the highest surface concentration of ligands that allows the glycerol to penetrate towards the Co surfaces, being around 3.50 nb L nm^{-2}, which corresponds to roughly half a dense monolayer (~6 nb L nm^{-2}). We then extract the corresponding carboxylate ligands surrounding the active site to build a small slab model of that site, which is tractable at the DFT level. Dehydrogenation pathways are then evaluated without and with ligands on both facets. The presence of carboxylate has a contrasting effect on the two facets. In contrast with our previous finding with organized acetate layers and isopropanol,[33] we found here that ligands are detrimental to the Co(11–20) activity but still boosting the Co(0001) activity. Besides, the predicted chemoselectivity is systematically in favour of DHA, in agreement with our previous observations comparing primary and secondary alcohols.[32]

2. Computational details

2.1. Molecular dynamics

Molecular mechanics molecular dynamics (MD) simulations were performed to simulate the adsorption of glycerol on Co(0001) and Co(11–20) surfaces with and without laurate ligands ($C_{11}H_{23}COO^*$). In the case with ligands, the ligand configuration on the cobalt surface, after a 1 ns equilibration from ref. 33, was used as the initial structure. Different ligand concentrations were tested, corresponding to different percentages of a monolayer (see ESI† section S2 for details).

All MD simulations were performed with a modified version of CP2K 9.16 using the smooth particle mesh Ewald summation with the alpha parameter set to 0.36 $Å^{-1}$. A grid resolution of approximately 1 point per Å of the unit cell length was employed. The standard scaling factors for 1–4 interactions were used: 0.5 for the van der Waals 1–4 interactions and 0.833 for the electrostatic 1–4 interactions. The GLJ cutoff was set to 10 Å. These simulations were conducted in the NVT ensemble employing a Nose–Hoover thermostat with a time constant of the thermostat chain of 200 fs at T = 448 K, which is the temperature employed by the experimental group for synthesizing the ligand-decorated Co nanoparticles.

The general AMBER force field (GAFF) was employed for organic molecules. The charge of Co atoms was set to zero and frozen during the MD simulation. To improve the description of the interaction of organic molecules with the cobalt surfaces, anisotropic attractive Gaussian potentials between surface cobalt atoms (Co) and oxygen (O) atoms of the organic molecules were added. There are two types of oxygen atoms: one from the laurate ligand ($C_{11}H_{23}COO^*$) and the other from the alcohol group of glycerol (atom type Oh). The parameters for the laurate ligand can be found in ref. 33, and the parametrization for Co–Oh can be found in ESI† section S1. Thanks to the use of the GLJ potential, the adsorption sites and the diffusion barriers between different sites on both cobalt surfaces are described correctly (Fig. S2 and S3†).

Thermodynamic integration (TI) was used to calculate the free energy barriers presented by different concentrations of ligands in relation to the transport of glycerol through the film. An optimized glycerol molecule was positioned 6 Å above the surface for the non-decorated surface and 22.2 Å above the decorated surface (5 Å above the ligand monolayer). A

constraint was applied to the *z*-position of the middle carbon atom (z), allowing the molecule to gradually penetrate the film with a velocity of 0.10 Å ps^{-1} until reaching the surface. The simulation took 250 ps with a time step of 0.50 fs. Various structures were obtained at different heights of the glycerol molecule, ranging from 22.20 Å to 1.50 Å above the surface. A total of 38 distinct distances were selected to sample the entire monolayer, with each distance representing a different z position. These structures served as the starting points for various simulations, during which the *Z*-coordinate of the middle carbon atom (z) in the molecule remained constant above the surface, allowing movement only in the *xy* plane for a duration of 800 ps, utilizing a constraining force. The time average of the constraining force was used to calculate the free energy $\Delta G(z)$ at a specific z position.

2.2. DFT computations

The Vienna *Ab initio* Simulation Package (VASP) computer program was used to perform periodic spin-polarized density functional theory (DFT) calculations.[43] The potential and the exchange correlation were calculated with the generalized gradient approximation (GGA), using the PBE functional[44] with dDsC dispersion correction.[45,46] A cut-off energy of 400 eV was applied to obtain a tight convergence of the plane-wave expansion. The projector augmented wave (PAW)[47,48] method was used to describe the electron–ion interactions. The SCF convergence criterion was set at 10^{-6} eV. A p(4 × 4) cell for the (0001) surface and a p(4 × 4) cell for the (11−20) surface were considered using a four-layer slab and over 15 Å of vacuum. For the Brillouin zone integration, a Monkhorst–Pack mesh of 3 × 3 × 1 *k*-points was used.[49] The two bottom layers of the slabs were kept fixed to the bulk truncated positions (with a Co–Co interatomic distance of 2.47 Å corresponding to the optimal hcp bulk, with the experimental value being equal to 2.51 Å) while the two upper layers were allowed to relax. 1.63 μ_B per Co atom was used as the initial magnetic moment value. Adsorption and reaction processes were realized on the upper surface of the slab. The structures were allowed to relax until the forces were lower than 0.015 eV $Å^{-1}$. Frequencies were computed numerically within the harmonic approximation. Transition states were optimized using a combination of CI-NEB[50,51] and the dimer method[52,53] and confirmed by the presence of a single imaginary frequency whose normal mode corresponds to the reaction coordinate.

Gibbs energies are derived from the electronic energies within the perfect gas model, the rigid rotator and harmonic oscillator approximations for molecules and the lattice gas for adsorbates. In other words, for molecules in the gas phase, Gibbs free energy G is calculated as follows:

$$G = E_{elec} + nK_BT + \mathrm{ZPE} - T \times (S_t + S_r + S_{vib}) \quad (1)$$

where E_{elec} is the electronic energy; n = 4 for non-linear molecules and n = 3.5 for linear molecules; K_B is the Boltzmann constant; T is the temperature, equal to 448 K; ZPE is the zero-point energy; and S_t, S_r, and S_{vib} are the translational, rotational, and vibrational entropy components, respectively. Adsorbates are considered to lose their rotational and translational degrees of freedom and have a diffusion energy that is higher than the thermal energy. Hence, their Gibbs free energies are considered as follows:

$$G_{ads/slab} = G_{slab} + \mathrm{ZPE} - T \times S_{vib} \quad (2)$$

where G_{slab} is the Gibbs free energy of a slab, $G_{ads/slab}$ is the Gibbs free energy of the species adsorbed on a slab and ZPE and S_{vib} are based on the harmonic vibration of the adsorbate. Frequencies lower than 50 cm^{-1} were neglected for all the entropy calculations.

The Gibbs free energy of adsorption (G_{ads}) for a given state was calculated as the difference between the energy of a molecule adsorbed on the surface and that of a molecule in the gas phase and of the surface, depending on the case. Negative energy means a stabilized adsorption.

$$G_{ads} = G_{ads/slab} - G_{slab} - G_{gas} \quad (3)$$

For both surfaces, CH_3COO ligands are co-adsorbed to mimic the presence of the longer chain carboxylate ligands on the NP surfaces. The position of the co-adsorbed ligands relative to glycerol was determined using molecular mechanics MD. For selected frames based on a cluster analysis of the trajectories (see below and Fig. S5(c) and (d)†), the model size was reduced while preserving the key features of MD geometries by cutting the simulation cell and replacing the long alkyl chain carboxylate ligands with CH_3COO* (acetate). The full protocol for structure selection and slab preparation is detailed in section S3 of the ESI.† Starting from 3.80 nb L nm^{-2} on Co(0001) and 3.50 nb L nm^{-2} on Co(11−20), this protocol includes 5 acetate ligands on the Co(0001)–p(5 × 5) and Co(11−20)–p(6 × 6) surfaces. On a selected case (the most abundant cluster on each surface, see ESI,† section S2), a lower coverage of 4 acetate ligands was also used to evaluate the coverage impact on the adsorption strength. In both cases (4 and 5 ligands), three hydrogen bonds were formed between glycerol and the ligands. The most stable configuration involved five ligands (Table S3†), which was used in most of the following studies.

The presence of acetate ligands decorating the surface induces a surface dipole. The dipole correction was included as a post-production check, analysing its influence on the energy of the key intermediate and transition of each path to check its influence on the resulting energy span. With the variation being minimal (see Table S10†), we present here the results obtained without this correction.

The energy span (δG) was calculated based on the energy span model (ESM) introduced by Kozuch and Shaik,[54] which enables the estimation of the turnover energy (TOF) from the free energy profile of the catalytic cycle. The model identifies the

TOF-determining transition state (TDTS) and the TOF-determining intermediate (TDI), and defines the energy span as:

$$\delta G = G_{TDTS} - G_{TDI} \quad (4)$$

when the TDTS appears after the TDI in the reaction sequence. If the TDTS precedes the TDI, the following expression is used:

$$\delta G = G_{TDTS} - G_{TDI} + \Delta G_{rxn} \quad (5)$$

where ΔG_{rxn} is the overall reaction free energy. In the case of GLY formation energy, it was set to zero for the energy span evaluation since it is predicted to be slightly endergonic at our DFT level at the chosen temperature.

3. Results and discussion

We started investigating the glycerol adsorption on both Co(0001) and Co(11–20) surfaces without and with ligands using molecular mechanics MD. This allowed us to build a model of the active site in the presence of ligands. We then computed the reaction pathways of glycerol dehydrogenation on bare surfaces and then decorated surfaces to predict how selectivity may be tuned in the presence of decorating ligands.

3.1. Glycerol adsorption: molecular mechanics and DFT study

The free energy profiles of glycerol diffusion through non-decorated and decorated cobalt surfaces were evaluated using molecular mechanics and thermodynamics integration, using the distance to the surface of the central carbon of glycerol. They are shown in ESI† Fig. S4. For the non-decorated surface (0 nb L nm^{-2}), the free energy profiles started from glycerol 6 Å above the surface, while for the decorated surface, the glycerol started from 22.20 Å above the surface. Glycerol started to interact with the ligand at around 17.20 Å. We observed that glycerol can diffuse through the ligand surface when the ligand concentration is below 3.80 nb L nm^{-2} and 3.50 nb L nm^{-2} for the Co(0001) and Co(11–20) surfaces, respectively. This corresponds to approximatively half of a dense monolayer. Otherwise, the free energy is positive, implying that the ligand concentration is too high to allow glycerol to diffuse. In other words, for the Co sites to be accessible and hence active, they need to be surrounded by a local coverage that is below half a dense monolayer. In other words, for the Co sites to be accessible—and therefore active—they must be surrounded by a local coverage below half a dense monolayer. This coverage is lower than the concentration generally found experimentally to stabilise unsupported metallic nanoparticles.[33] Due to their similar concentrations and free energy profiles (Fig. 1), 3.80 nb L nm^{-2} and 3.50 nb L nm^{-2} were chosen for the decorated Co(0001) and Co(11–20) surfaces, respectively (Fig. 1).

Adsorption free energy of glycerol on bare Co(11–20) is around −1.50 eV, while on Co(0001) it is around −1.00 eV. In other words, glycerol adsorbs more strongly on the open facet Co(11–20) in the absence of long-chain carboxylate ligands at the molecular mechanics level. In contrast, when considering decorated Co(0001) and Co(11–20), the adsorption free energy of glycerol is quite similar, at −0.95 eV and −0.84 eV, respectively, and weaker than in the absence of ligands. This weaker adsorption free energy in the presence of ligands results from the loss of stabilizing Co–O bonds (from 3 Co–O bonds when glycerol is chemisorbed on the bare surfaces to 2 on average on the decorated surface) that is not compensated by H-bonding.

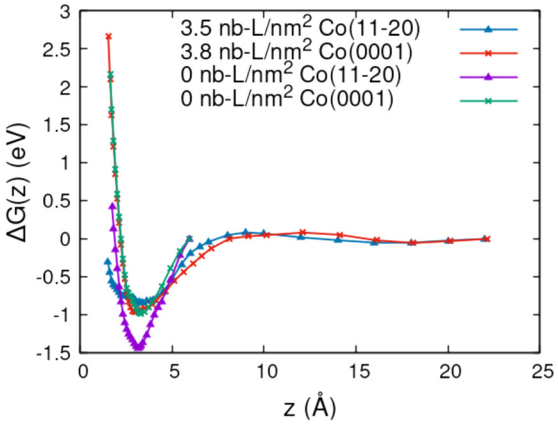

Fig. 1 Free energy profiles $\Delta G(z)$ as a function of the distance of the middle carbon to the surface Z, computed with TI for non-decorated and decorated cobalt surfaces Co(0001) and Co(11–20).

To generate initial configurations for DFT calculations, we carefully analysed MM MD trajectories starting with the central C of glycerol at 3 Å which corresponds to the minimum of the free energy adsorption profile on each surface. The time evolution of the distances to the surface of the three O atoms (O_1 and O_3 are the terminal oxygen atoms, and O_2 is the central oxygen atom) and the central C atom (C_2) is plotted in Fig. S5.†

On both non-decorated surfaces, all three O atoms are adsorbed on the surface at a distance around 2.2 Å (Fig. S5(a) and (b)†) during classical MD trajectories ran at 448 K. In contrast, the DFT optimal structures of chemisorbed glycerol (Fig. 2) show only two oxygen atoms adsorbed on the sites of Co on both surfaces, Co(0001) and Co(11–20). This small discrepancy can be related to temperature effects. In agreement with the free energy adsorption profiles obtained at the MM level (Fig. 1), the Gibbs energy of adsorption is more negative on Co(11–20) than on Co(0001) (G_{ads} = −0.38 eV *vs.* G_{ads} = −0.08 eV).

On decorated surfaces, the number of Co–O_{gly} bonds varies along the MD trajectories (Fig. S5(c) and (d)†). In order to analyse these trajectories in detail, the structures were grouped into five clusters based on the number and the nature of glycerol oxygens located at a distance from the Co surface below a cut-off distance of 2.2 Å:

- Cluster_O_t: one terminal O (O_1 or O_3).
- Cluster_O_2: the central oxygen O_2
- Cluster_O_1–O_3: the two terminal oxygens (O_1 and O_3)

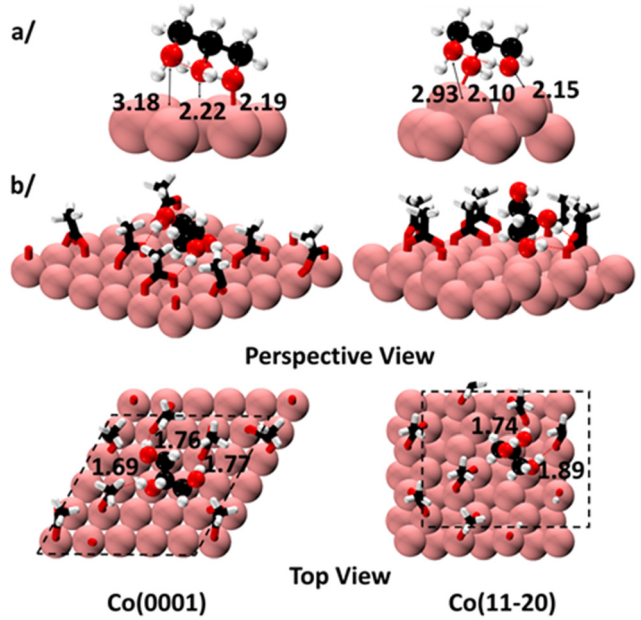

Fig. 2 Most stable conformations of glycerol on the (a) bare Co(0001) and Co(11–20) surfaces, and (b)on decorated Co(0001) and Co(11–20) surfaces (perspective and top views are presented, showing only the top layers of the metallic slabs). Black, red, white and pink correspond to C, O, H and Co atoms, respectively. Hydrogen bonds are represented in dashed red lines. All bond lengths are expressed in Å.

• Cluster_O_t–O_2: one terminal oxygen (O_1 or O_3) and the central oxygen (O_2)

• Cluster_O_1–O_2–O_3: the three oxygens of glycerol

Then, several representative structures were selected from each of the five MD-derived clusters to construct DFT models of glycerol chemisorbed on Co(0001)–p(5 × 5) and Co(11–20)–p(6 × 6) surfaces decorated with five acetate ligands as detailed in the computational details. The stability of the most sable DFT models obtained for each cluster is reported in Tables S4 and S5.†

On decorated Co(0001), the most abundant cluster is Cluster_O_2 (33.7%), followed by Cluster_O_t (22.1%), showing that glycerol adsorption is strongly dominated by structures where glycerol is bonded to the Co surface through only one oxygen. Moving to the DFT models derived from selected representative structures of the MM trajectory, we found that the most stable conformer corresponds to the most abundant classified cluster from the classical MD trajectory (Cluster_O_2 at 33.7%, see Fig. S6†). The corresponding structure is shown in Fig. 2b. Glycerol is still bonded only through the central hydroxyl, with a Co–$O_{central}$ distance of 2.19 Å. Even if the presence of ligands limits the number of glycerol/Co interactions, the adsorption is stronger on the decorated Co(0001) (−1.60 eV). This stronger adsorption is likely related to the presence of three hydrogen bonds linking each hydroxyl group of the chemisorbed glycerol with a different carboxylate ligand. These H-bonds are quite strong given their short distances ($d_{H\cdots O}$ = 1.77 Å, 1.76 Å and 1.69 Å, see Fig. 2).

On decorated Co(11–20), the analysis of the MD shows five clusters of almost equivalent weight (Fig. S6†), with a slight preference for the monodentate adsorption modes (Cluster_O_2 (25%) and Cluster_O_t (19.6%)). Models of the glycerol adsorption site were again extracted to optimize the adsorption structures at the DFT level. The most stable conformer obtained at the DFT level was derived from Cluster_O_t (Table S4†). One terminal oxygen is bonded to the surface ($d_{Ot–Co}$ = 2.05 Å) building a hydrogen bond with the ligands surrounding ($d_{Ot–H}$ = 1.74 Å) whereas the two other oxygens are farther from the surface. The central oxygen still maintains a hydrogen bond with the surrounding ligands ($d_{Oc–H}$ = 1.89 Å). Similar to the Co(0001), the presence of ligands increases the adsorption strength (G_{ads} = −0.73 eV). The adsorption free energy of glycerol on decorated Co(0001) and Co(11–20) are quite similar (−0.79 eV and −0.73 eV respectively), in line with the free energy simulations at the MM level (Fig. 1).

In conclusion, the presence of carboxylate ligands affects the adsorption strength and structure of glycerol on Co(0001) and Co(11–20). A careful analysis of the MM-MD trajectory allowed us to build models of the active site on decorated Co(0001) and Co(11–20) to be used at the DFT level. Both approaches (MM-MD and static DFT) provided similar conclusions: in the presence of ligands, the stabilization by adsorption is weaker and monodentate adsorption is favored rather than multidentate adsorption. Given the change in adsorption modes and adsorption energy observed for glycerol in the presence of ligands, they are expected to tune the reaction profiles of the dehydrogenation of terminal *vs.* central hydroxyl groups of glycerol, an effect that will be explored in detail in the next part.

3.2. Glycerol dehydrogenation over bare Co(0001) and Co(11–20)

Gibbs free energy diagram. Alcohol dehydrogenation catalysed by metal surfaces can follow two pathways: the alkoxy pathway which starts with the scission of the O–H bond, or the hydroxyl alkyl pathway which starts with the scission of the C–H bond. According to the literature, the alkoxy pathway is preferred for the dehydrogenation of alcohols on cobalt NPs.[33,55–58] Still, two alkoxy pathways are in competition for the glycerol dehydrogenation, depending on the hydroxyl group that undergoes dehydrogenation. Dehydrogenation of the terminal OH (OH_t) yields glyceraldehyde (GLYA) while dehydrogenation of the central OH (OH_c) yields dihydroxyacetone (DHA). The Gibbs energy profiles corresponding to these two alkoxy pathways are provided in Fig. 3 on Co(0001) using a black line and on Co(11–20) using a grey line. The energy barriers and energy spans are collected in Table 1.

Importantly, the formation of DHA is more exergonic than the formation of GLYA (−0.21 eV *vs.* +0.10 eV) which is in line with the known thermodynamics of dehydrogenation of primary *vs.* secondary alcohols but also with other studies on

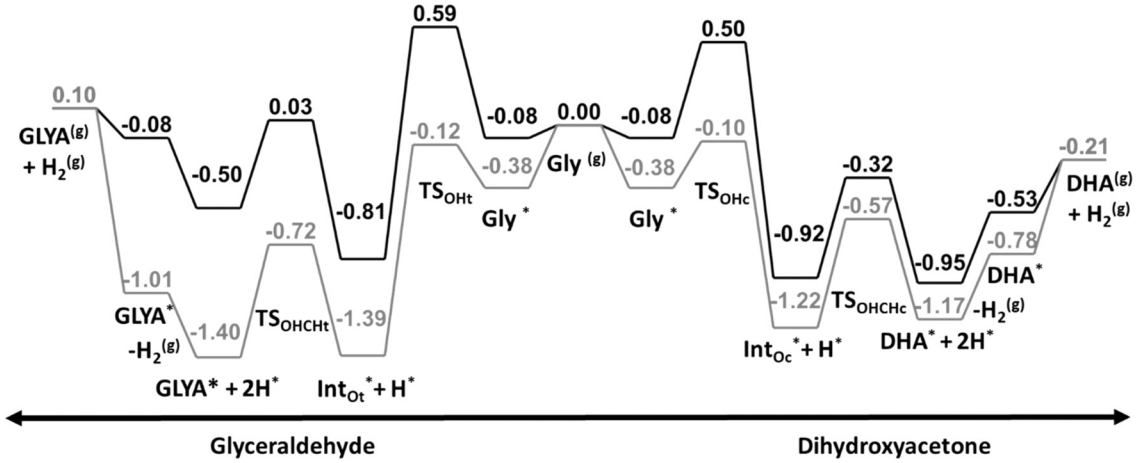

Fig. 3 Gibbs free energy profiles (in eV) for glycerol (Gly) dehydrogenation *via* the alkoxy pathway on the Co(0001) (black lines) and on the Co(11–20) (grey lines) at T = 448 K. On the left is the pathway leading to glyceraldehyde (GLYA) and on the right is the pathway leading to dihydroxyacetone (DHA). The reference energy is isolated glycerol and the isolated surface. (*) means adsorbed species.

Table 1 A comparative table of the different energy barriers of transition states and relative energy spans (eV) on the pristine and decorated (0001) and (11–20) cobalt surfaces

		Surface			
Pathway	TS	Co(0001)	Decorated Co(0001)	Co(11–20)	Decorated Co(11–20)
Dihydroxyacetone	TS_{OH}	E_a = 0.58	E_a = 0.77	E_a = 0.28	E_a = 0.49
	TS_{OHCH}	E_a = 0.67	E_a = 0.75	E_a = 0.65	E_a = 1.08
Glyceraldehyde	TS_{OH}	E_a = 0.67	E_a = 0.55	E_a = 0.26	E_a = 0.55
	TS_{OHCH}	E_a = 0.84	E_a = 0.99	E_a = 0.67	E_a = 1.43
		Energy span (eV)			
Dihydroxyacetone		E_{span} = 1.24	E_{span} = 0.84	E_{span} = 1.01	E_{span} = 1.17
Glyceraldehyde		E_{span} = 1.40	E_{span} = 1.12	E_{span} = 1.28	E_{span} = 1.43

glycerol.[21,25] The comparison of the Gibbs free energy profiles shows that intermediates and transition states are more stabilized on Co(11–20) than on Co(0001). This can be directly related to the lower coordination number of surface Co on the more open facet Co(11–20).[33] Still, the activity on Co(11–20) may be limited by a too strong adsorption and the selectivity may depend on the nature of the facet.

On Co(0001) (Fig. 3, black line), the glycerol chemisorption is slightly exergonic (G_{ads} = −0.08 eV) leading to a short contact between the alcohol and the surface catalyst. The formation of the alkoxy intermediates (Int_{Oc} and Int_{Ot}) is exergonic. The adsorption of the alkoxy on a ternary site is strongly stabilized by three Co–O bonds (Fig. 4). Int_{Oc} is 0.10 eV more stable than Int_{Ot}. The two activation barriers are lower on the DHA pathway than on the GLYA pathway: E_a = 0.58 eV *vs.* E_a = 0.67 eV for the first OH bond scission and E_a = 0.60 eV *vs.* E_a = 0.84 eV for the second CH bond scission. Last, the desorption of the products is easy, almost athermic. In short, the reaction is limited by the stability of the alkoxy intermediate and is strongly in favor of the formation of DHA with lower activation barriers and a greater stability of the Int_{Oc} intermediate. This selectivity towards DHA is also clearly shown by the difference in the energy span (1.40 eV for GLYA *vs.* 1.24 eV for DHA, reported in Table 1).

On Co(11–20) (Fig. 3, grey lines), the glycerol chemisorption is exergonic (G_{ads} = −0.38 eV). The formation of the alkoxy intermediates is also strongly exergonic; in contrast with the profiles found on Co(0001), Int_{Ot} is more stable than Int_{Oc} by 0.17 eV. This can be related to the structures (Fig. 5): Int_{Ot} is bonded to the surface through three hydroxyl groups ($d_{O–Co}$ = 1.90 Å, 2.09 Å, 2.25 Å) while Int_{Oc} is only bonded by two hydroxyl groups (its central oxygen, $d_{O–Co}$ = 1.91 Å and one of the terminal oxygens, $d_{O–Co}$ = 2.13 Å). The activation barriers are similar on both pathways: the OH bond scission is easy, with a very small barrier (E_a ~0.26–0.28 eV) while the C–H bond scission is the limiting step with a barrier of 0.65 eV for CH_c and 0.67 eV for CH_t. With a more stable intermediate, and a less stable product (GLYA), the production rate of the GLYA pathway is limited by the successive dehydrogenation of Int_{Ot} and desorption of the two products, H_2 and GLYA. This yields an energy span of 1.28 eV that is higher than the one found for the production of DHA (1.01 eV). In other words, the Co(11–20) surface is also selective towards DHA, but to a

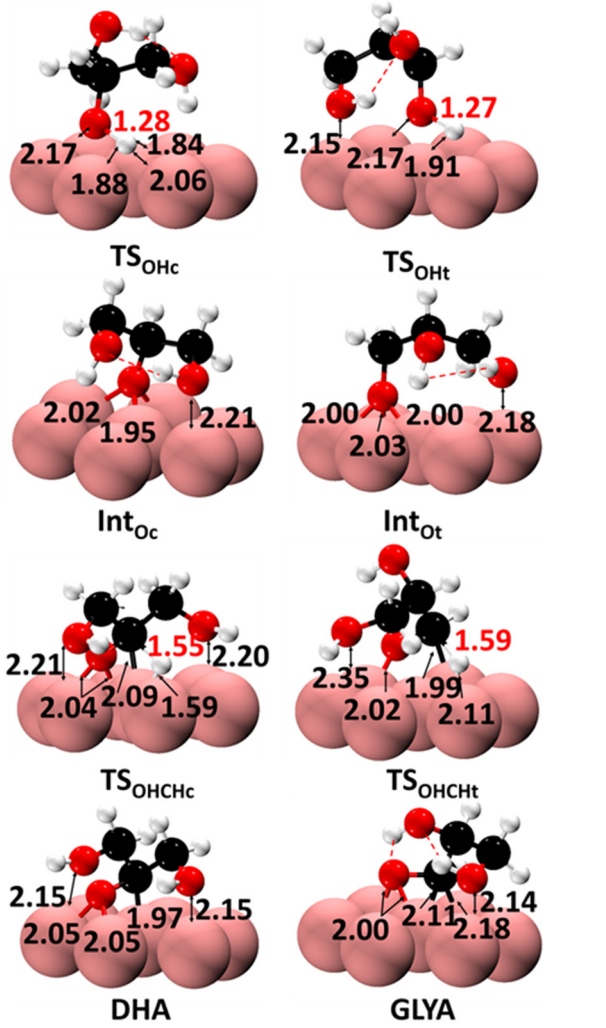

Fig. 4 Structures of intermediates, products and transition states for the first and the second steps of the glycerol dehydrogenation reaction on bare Co(0001). Pink, black, red and white correspond to Co, C, O and H atoms, respectively. Dashed red lines represent hydrogen bonds (O···H distance below 2.02 Å). Values in red in the TSs represent the values of the OH or CH bond distance scission, respectively. All bond lengths are expressed in Å.

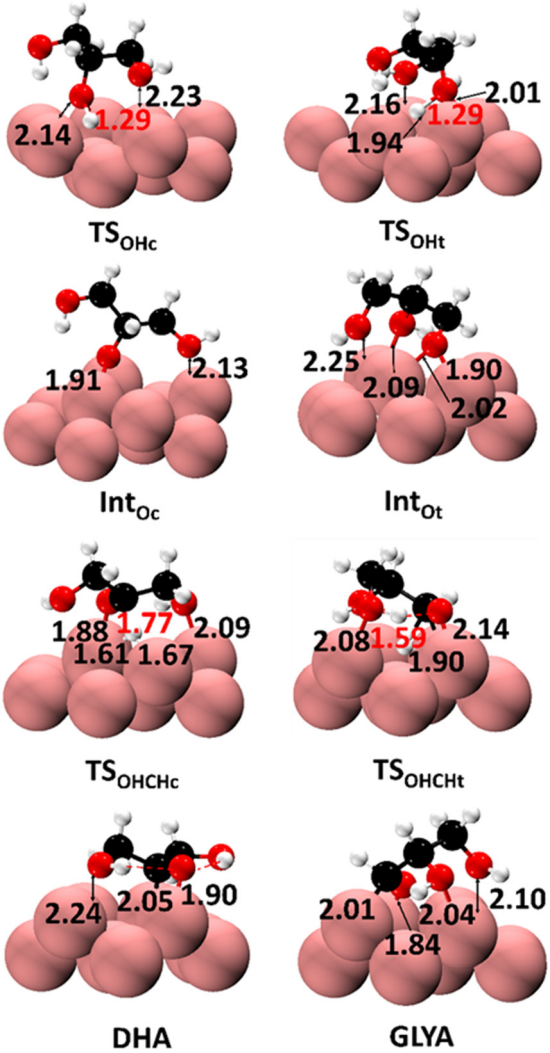

Fig. 5 Structures of intermediates, products and transition states for the first and the second steps of the glycerol dehydrogenation reaction on the bare Co(11–20) surface. Pink, black, red and white correspond to Co, C, O and H atoms, respectively. Dashed red lines represent hydrogen bonds (O···H distance below 2.02 Å). Values in red in the TSs represent the values of the OH or CH bond distance scission, respectively. All bond lengths are expressed in Å.

lesser extent than Co(0001). In addition, this more open surface is also more active since the energy spans of both pathways are lowered by at least 0.16 eV (Table 1). This agrees with what is found for iPrOH dehydrogenation.[33]

3.3. Glycerol dehydrogenation over the decorated Co(0001) and Co(11–20) surfaces

Using the models of the decorated Co(0001) and decorated Co(11–20) surfaces (see section 3.1), we investigated how carboxylate ligands may tune the reaction profile of the glycerol dehydrogenation and the resulting activity and selectivity.

We first compared the H-transfer to the metallic surface with the transfer to an oxygen of a nearby carboxylate ligand. On the one hand, the chemisorbed H atom can still bind in an fcc site of Co(0001) and a bridge site of Co(11–20) despite the crowdedness of the metallic surface, but those bonds are weaker than those on pristine Co surfaces: the H_2 adsorption energy on the decorated surface is weakened, approximately halved. On the other hand, the transfer of a H atom to a ligand results in the loss of a strong Co–O bond. This is why the H-transfer to the surface is still favoured thermodynamically over the transfer to an acetate by around 0.90 eV on decorated Co(0001) and 0.96 eV on decorated Co(11–20). Therefore, in the following text, we have systematically considered H-transfer to the metallic surface and subsequent recombination as H_2 as the dominant mechanism of glycerol dehydrogenation. The corresponding Gibbs energy profiles are shown in Fig. 6 and the structures are in Fig. 7 and 8. The energy barriers and energy spans are collected in Table 1.

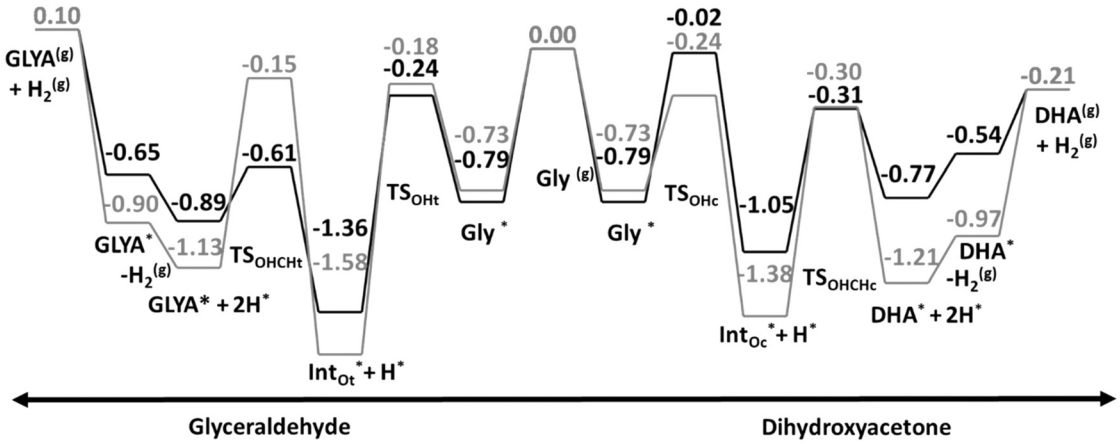

Fig. 6 Gibbs free energy (eV) diagram of glycerol dehydrogenation into the DHA product (right side) and GLYA product (left side) at T = 448 K on both decorated Co(0001) (black lines) and Co(11–20) (grey lines) surfaces.

On the decorated Co(0001) (Fig. 6, black lines), the terminal O–H bond breaks more easily than the central one, with an activation barrier that is 0.20 eV lower. In addition, the resulting alkoxy intermediate (Int_{Ot}) is more stable by 0.31 eV. This is in stark contrast with the relative OH scission barriers and Int_O stabilities found on the pristine Co(0001) surface. This can be related to the catalytic pocket formed by carboxylate ligands. The chemisorption of glycerol is strongly stabilized through 3 H-bonds but one of them needs to be broken to reach the TS_{OH} transition states. This results in a barrier up to 0.77 eV for the scission of OH_c. However, these transition states are lying at a noticeable lower energy level relative to the reactant on the decorated Co(0001) than on the pristine Co(0001) (*e.g.* −0.02 eV *vs.* −0.24 eV for TS_{OHc}), thanks to the greater interaction with the catalytic site. Similar to what is found on pristine Co(0001), the alkoxy intermediates are chemisorbed in a hollow site, but they also build an H-bond network with the carboxylate ligands of the catalytic pocket. The two H-bonds are stronger in Int_{Ot} than in Int_{Oc} (with distances of 1.80 Å and 1.78 Å *vs.* 2.07 Å and 1.90 Å, Fig. 7 and Table S9†) which results in a greater stability of Int_{Ot}. While the C–H dissociation was easy on the pristine Co(0001) surface, it is now sterically hindered by the presence of the carboxylate ligands. The C–H scission barrier rises to 0.75 eV on the DHA pathway and even to 0.99 eV on the GLYA pathway. The resulting products are quite stabilized on the surface and their desorption is also more demanding than on the pristine Co(0001) surface. As a result, the production of GLYA on the decorated Co(0001) is limited by the enhanced stability of Int_{Ot} which shows an energy span of 1.12 eV. Producing DHA is easier (an energy span of 0.84 eV) and its rate is controlled by the two successive steps with barriers of 0.77 eV and 0.75 eV. Despite strong modifications in the stabilization of intermediates and barriers, the selectivity of the decorated Co(0001) is similar to the one found on the pristine Co(0001) surface, with DHA being the favoured product. Importantly, kinetics is even enhanced with a lower energy span (0.84 eV *vs.* 1.24 eV), despite the rise in the first O–H scission barrier. This can be directly ascribed to the greater stabilization of the chemisorbed glycerol and

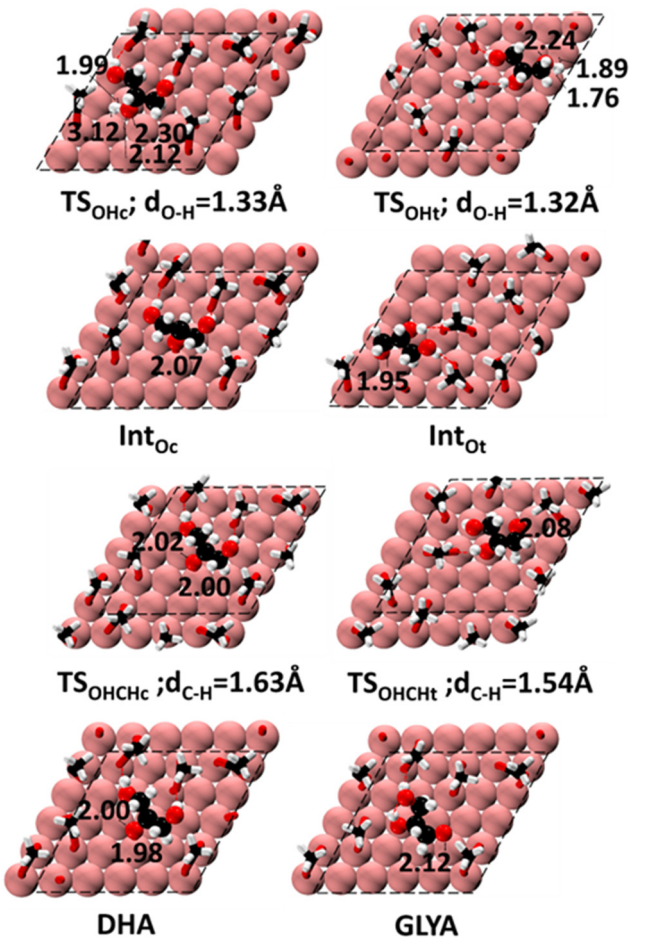

Fig. 7 Structures of intermediates, products and transition states for the first and the second steps of the glycerol dehydrogenation reaction on the bare Co(0001) surface. Pink, black, red and white correspond to Co, C, O and H atoms, respectively. Dashed red lines represent hydrogen bonds (O···H distance below 2.02 Å). All bond lengths are expressed in Å.

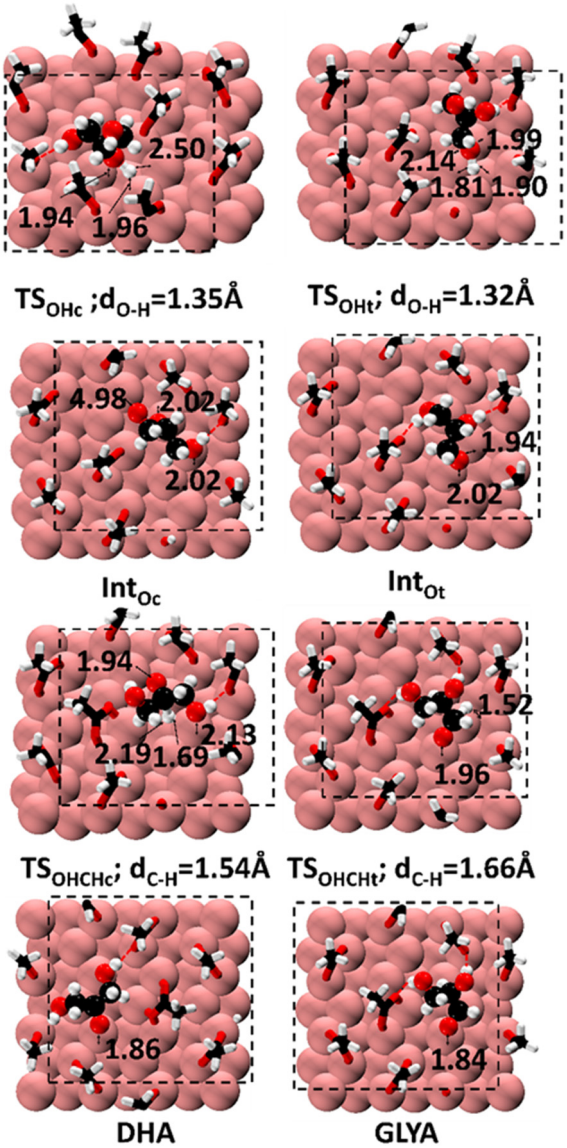

Fig. 8 Structures of intermediates, products and transition states for the first and the second steps of the glycerol dehydrogenation reaction on the bare Co(11–20) surface. Pink, black, red and white correspond to Co, C, O and H atoms, respectively. Dashed red lines represent hydrogen bonds (O···H distance below 2.02 Å). All bond lengths are expressed in Å.

the TS_{OHc} relative to the free glycerol, an effect that is provided by the catalytic pocket.

On decorated Co(11–20) (Fig. 6, grey line and Fig. 8), the combination of two effects results in a very strong stabilization of Int_{Oc} (−1.38 eV) and Int_{Ot} (−1.58 eV). First, the intermediates are more strongly bonded to the decorated surface Co(11–20) than on the decorated Co(0001) due to the lower coordination of the Co surface atoms, an intrinsic property of the Co(11–20) surface. Second, all intermediates and transition states are stabilized by the catalytic pocket, similar to what is observed on the decorated Co(0001). This second effect is limited by higher geometrical constrains of that surface where the ligands can only diffuse along the Co zigzag rows and not in the perpendicular direction.[42] This tends to limit the number of H-bonds that the glycerol, the transition states and the intermediates can build along the reaction pathways. The number of H-bonds is typically limited to 1 on Co(11–20) while it easily reached 2 on decorated Co(0001) (see Table S9†). This has strong consequences on the relative stability of the intermediates and transition states along the two pathways. In contrast with the Co(0001) surface, the inclusion of carboxylate decoration deactivates the Co(11–20) surface.

On the GLYA pathway, Int_{Oc} is strongly stabilized but the following transition state (TS_{OHcCHc}) is hindered by the presence of the ligands around the catalytic pocket. The resulting activation barrier (1.43 eV) limits considerably the formation of GLYA. On the DHA pathway, we observe a small stabilization of TS_{OHCHc} by the ligand pocket. Thus, the subsequent C–H scission barrier (1.08 eV) is clearly lower than that on the terminal position (1.43 eV), and DHA is the most favoured product on decorated Co(11–20). However, this type of site is not as active as the other ones considered in this study. The presence of ligands induces a rise in the energy span of both pathways reaching 1.17 eV and 1.43 eV, compared with the decorated Co(0001) and also with the pristine Co(11–20), making the decorated Co(11–20) surface clearly less active than all the other cases we investigated. This deactivation is still occurring when using one less ligand to decorate the surface. The corresponding profiles have been recomputed and are shown in Fig. S12.† The energy span is still high, reaching 1.13 eV for DHA and 1.42 eV for GLYA on the Co(11–20) decorated with 4 ligands rather than 5.

4. Conclusion

Unsupported Co nanoparticles stabilized using long-chain carboxylate ligands can be successfully used as catalysts to perform alcohol dehydrogenation yielding carbonyl derivatives and H_2. Combining molecular mechanics and DFT, we investigated here the dehydrogenation reaction of glycerol into dihydroxyacetone (DHA), glyceraldehyde (GLYA) and H_2 to predict how the presence of long-chain carboxylate ligands may affect the activity and selectivity.

To investigate the adsorption of glycerol at the Co/carboxylate interface, we benefited from a bespoke force field, which is able to properly describe Co–O interactions (Co/carboxylate and Co/glycerol). Using thermodynamical integration at the MM level, we then obtained the adsorption free energy profile as a function of the surface concentration and the type of the surface, with the Co(0001) and Co(11–20) being the two most exposed surfaces of the most efficient Co nanoparticles that exhibit a nanorod shape. A concentration of 3.5–3.8 nb L nm^{-2} appears as the upper threshold that is slightly above half a dense monolayer.

At that ideal concentration, long MM trajectories of chemisorbed glycerol were ran at the typical reaction temperature of 448 K. On pristine surfaces, glycerol binds through its three O atoms, while on the decorated surfaces, the number of Co–O_{gly} bonds varies. A cluster analysis split

shows that monodentate adsorption is clearly dominant. Model structures using shorter chains and smaller surface slabs were then extracted out of these trajectories to be used at the DFT level. The most stable conformer of glycerol chemisorbed on the decorated surface is also found to be monodentate, through the central hydroxyl on Co(0001) and a terminal hydroxyl on Co(11–20). In contrast, glycerol is chemisorbed in a bidentate mode on both bare Co surfaces. The presence of decorating ligands modifies the glycerol adsorption mode, and it also tunes the chemisorption strength, especially on Co(11–20) where the carboxylate cannot adapt as easily as on the Co(0001) due to the stronger corrugation.

The selectivity and activity of the glycerol dehydrogenation is certainly also modified by the presence of ligands. DHA is the thermodynamic product. According to the Gibbs energy reaction profiles computed at the DFT level, it is also the product that is easier to obtain on all four surfaces (bare and decorated Co(0001) and Co(11–2)). When considering the DHA route, Co(11–20) is more productive than Co(0001) in the absence of carboxylate due to lower coordinated Co surface atoms. However, when moving to the decorated surface, the trend is reversed. The activity of a given active site of Co(0001) is increased, with a marked decrease in the energy span of 0.40 eV to produce DHA, whereas the activity of Co(11–20) tends to decrease, with an increase in the energy span of 0.16 eV. This contrasting effect can be related to an over-stabilization of the alkoxy intermediate on decorated Co(11–20). In other words, the presence of decorating ligands can tune the structure sensitivity of a reaction and modify the nature of the most active facet. In our specific case, a platelet shape, exposing mainly the Co(0001) surface with a coverage as low as possible, is predicted to be more active than rods that expose mainly Co(11–20), in contrast with what has been found on monoalcohols. These theoretical predictions are expected to be tested by our experimental partners as part of the ongoing collaborative project. This forthcoming validation will further strengthen the synergy between theory and experiment, contributing to the rational design of more selective catalytic systems.

Data availability

The data supporting this article have been included as part of the ESI.†

Conflicts of interest

There are no conflicts to declare.

Acknowledgements

The work was done as a part of the ANR GLYNANO project funded by the French National Research Agency (ANR-21-CE43-0016). The authors acknowledge the CBPsmn mesocenter in Lyon for CPU time and assistance (CPER/SYSPROD 2015–2022 project no. 2019-AURA-P5B and AXELERA Pôle de compétitivité).

References

1 A. Friedrich and S. Schneider, Acceptorless Dehydrogenation of Alcohols: Perspectives for Synthesis and H 2 Storage, *ChemCatChem*, 2009, **1**, 72–73.
2 J. Choi, A. H. R. MacArthur, M. Brookhart and A. S. Goldman, Dehydrogenation and Related Reactions Catalyzed by Iridium Pincer Complexes, *Chem. Rev.*, 2011, **111**, 1761–1779.
3 T. C. Johnson, D. J. Morris and M. Wills, Hydrogen generation from formic acid and alcohols using homogeneous catalysts, *Chem. Soc. Rev.*, 2010, **39**, 81–88.
4 R. H. Crabtree, Transfer Hydrogenation with Glycerol as H-Donor: Catalyst Activation, Deactivation and Homogeneity, *ACS Sustainable Chem. Eng.*, 2019, **7**, 15845–15853.
5 N. Gupta, O. Khavryuchenko, A. Villa and D. Su, Metal-Free Oxidation of Glycerol over Nitrogen-Containing Carbon Nanotubes, *ChemSusChem*, 2017, **10**, 3030–3034.
6 S.-S. Liu, K.-Q. Sun and B.-Q. Xu, Specific Selectivity of Au-Catalyzed Oxidation of Glycerol and Other C 3 -Polyols in Water without the Presence of a Base, *ACS Catal.*, 2014, **4**, 2226–2230.
7 K. Chung, S. M. Banik, A. G. De Crisci, D. M. Pearson, T. R. Blake, J. V. Olsson, A. J. Ingram, R. N. Zare and R. M. Waymouth, Chemoselective Pd-Catalyzed Oxidation of Polyols: Synthetic Scope and Mechanistic Studies, *J. Am. Chem. Soc.*, 2013, **135**, 7593–7602.
8 Y. Wang, D. Yuan, J. Luo, Y. Pu, F. Li, F. Xiao and N. Zhao, The effects of calcination temperature of support on Au/CuO-ZrO2 catalysts for oxidation of glycerol to dihydroxyacetone, *J. Colloid Interface Sci.*, 2020, **560**, 130–137.
9 J. Feng, W. Xiong, H. Ding and B. He, Hydrogenolysis of glycerol over Pt/C catalyst in combination with alkali metal hydroxides, *Open Chem.*, 2016, **14**, 279–286.
10 F. Auneau, C. Michel, F. Delbecq, C. Pinel and P. Sautet, Unravelling the Mechanism of Glycerol Hydrogenolysis over Rhodium Catalyst through Combined Experimental–Theoretical Investigations, *Chem. – Eur. J.*, 2011, **17**, 14288–14299.
11 A. El Roz, P. Fongarland, F. Dumeignil and M. Capron, Glycerol to Glyceraldehyde Oxidation Reaction Over Pt-Based Catalysts Under Base-Free Conditions, *Front. Chem.*, 2019, **7**, 156.
12 M. Sherbi, A. Wesner, V. K. Wisniewski, A. Bukowski, H. Velichkova, B. Fiedler and J. Albert, Superior CNT-supported bimetallic RuCu catalyst for the highly selective hydrogenolysis of glycerol to 1,2-propanediol, *Catal. Sci. Technol.*, 2021, **11**, 6649–6653.
13 Q. Sun, S. Wang and H. Liu, Selective Hydrogenolysis of Glycerol to Propylene Glycol on Supported Pd Catalysts: Promoting Effects of ZnO and Mechanistic Assessment of Active PdZn Alloy Surfaces, *ACS Catal.*, 2017, **7**, 4265–4275.

14 D. B. Lao, A. C. E. Owens, D. M. Heinekey and K. I. Goldberg, Partial Deoxygenation of Glycerol Catalyzed by Iridium Pincer Complexes, *ACS Catal.*, 2013, **3**, 2391–2396.
15 D. Ainembabazi, K. Wang, M. Finn, J. Ridenour and A. Voutchkova-Kostal, Efficient transfer hydrogenation of carbonate salts from glycerol using water-soluble iridium N-heterocyclic carbene catalysts, *Green Chem.*, 2020, **22**, 6093–6104.
16 H. Narjinari, S. Dhole and A. Kumar, Acceptorless or Transfer Dehydrogenation of Glycerol Catalyzed by Base Metal Salt Cobaltous Chloride – Facile Access to Lactic Acid and Hydrogen or Isopropanol, *Chem. – Eur. J.*, 2023, **30**, e202302686.
17 A. Behr, J. Eilting, K. Irawadi, J. Leschinski and F. Lindner, Improved utilisation of renewable resources: New important derivatives of glycerol, *Green Chem.*, 2008, **10**, 13–30.
18 D. I. Enache, J. K. Edwards, P. Landon, B. Solsona-Espriu, A. F. Carley, A. A. Herzing, M. Watanabe, C. J. Kiely, D. W. Knight and G. J. Hutchings, Solvent-Free Oxidation of Primary Alcohols to Aldehydes Using Au-Pd/TiO_2 Catalysts, *Science*, 1979, **2006**(311), 362–365.
19 R. Ciriminna, A. Fidalgo, L. M. Ilharco and M. Pagliaro, Dihydroxyacetone: An Updated Insight into an Important Bioproduct, *ChemistryOpen*, 2018, **7**, 233–236.
20 L. Bricotte, K. Chougrani, V. Alard, V. Ladmiral and S. Caillol, Dihydroxyacetone: A User Guide for a Challenging Bio-Based Synthon, *Molecules*, 2023, **28**, 2724.
21 C. Crotti, J. Kašpar and E. Farnetti, Dehydrogenation of glycerol to dihydroxyacetone catalyzed by iridium complexes with P–N ligands, *Green Chem.*, 2010, **12**, 1295.
22 S. Kostera and L. Gonsalvi, Sustainable Hydrogen Production by Glycerol and Monosaccharides Catalytic Acceptorless Dehydrogenation (AD) in Homogeneous Phase, *ChemSusChem*, 2024, **18**, e202400639.
23 E. Boccalon, G. Menendez Rodriguez, C. Trotta, F. Ruffo, C. Zuccaccia and A. Macchioni, Acceptorless Dehydrogenation of Glycerol Catalysed by Ir(III) Complexes with Carbohydrate-Functionalised Ligands: A Sweet Pathway to Produce Hydrogen and Lactic Acid, *Eur. J. Inorg. Chem.*, 2024, **27**, e202400507.
24 R. C. R. dos Santos, M. J. da Silva Júnior, G. L. Nunes and A. Valentini, Effect of Cu and Sb active sites on the acid–base properties and reactivity of hydrated alumina for glycerol conversion by dehydrogenation and dehydration reactions, *Catal. Sci. Technol.*, 2023, **13**, 4223–4245.
25 M. Valter, E. C. dos Santos, L. G. M. Pettersson and A. Hellman, Selectivity of the First Two Glycerol Dehydrogenation Steps Determined Using Scaling Relationships, *ACS Catal.*, 2021, **11**, 3487–3497.
26 N. A. Karim, M. S. Alias and S. K. Kamarudin, The mechanism of the water dissociation and dehydrogenation of glycerol on Au (111) and PdAu alloy catalyst surfaces, *Int. J. Hydrogen Energy*, 2021, **46**, 30937–30947.
27 W. Wang, H. Ma, J. Zhu, F. Zhou, H. Xu and D. Cheng, Can ZnO/Cu catalyst provide promising activity for glycerol direct dehydrogenation? A combined density functional theory and coverage-dependent microkinetics study, *J. Catal.*, 2024, **439**, 115786.
28 K. Wang, J. Horlyck, N. An and A. Voutchkova-Kostal, Homogeneous vs. heterogeneous catalysts for acceptorless dehydrogenation of biomass-derived glycerol and ethanol towards circular chemistry, *Green Chem.*, 2024, **26**, 3546–3564.
29 B. Liu and J. Greeley, A density functional theory analysis of trends in glycerol decomposition on close-packed transition metal surfaces, *Phys. Chem. Chem. Phys.*, 2013, **15**, 6475.
30 B. Azeredo, T. Ben Ghzaiel, N. Huang, K. Kaźmierczak, W. Shen, G. Wang, D. Schaming, P. Beaunier, P. Decorse, N. Perret, J. Peron, M. Giraud, C. Michel, L. Sicard and J.-Y. Piquemal, Co–Ru Nanoalloy Catalysts for the Acceptorless Dehydrogenation of Alcohols, *ACS Appl. Nano Mater.*, 2022, **5**, 5733–5744.
31 N. Huang, C. Hammed, G. Wang, S. Nowak, P. Decorse, D. Schaming, A. Gannouni, W. Najjar, C. Michel, L. Sicard and J. Piquemal, Copper-Cobalt Bimetallic Nanoparticles for the Acceptorless Dehydrogenation of Alcohols: A Combined Experimental and Theoretical Study, *ChemNanoMat*, 2024, **10**, e202400259.
32 A. Viola, J. Peron, K. Kazmierczak, M. Giraud, C. Michel, L. Sicard, N. Perret, P. Beaunier, M. Sicard, M. Besson and J. Y. Piquemal, Unsupported shaped cobalt nanoparticles as efficient and recyclable catalysts for the solvent-free acceptorless dehydrogenation of alcohols, *Catal. Sci. Technol.*, 2018, **8**, 562–572.
33 K. Kaźmierczak, R. K. Ramamoorthy, A. Moisset, G. Viau, A. Viola, M. Giraud, J. Peron, L. Sicard, J. Y. Piquemal, M. Besson, N. Perret and C. Michel, Importance of the decoration in shaped cobalt nanoparticles in the acceptorless secondary alcohol dehydrogenation, *Catal. Sci. Technol.*, 2020, **10**, 4923–4937.
34 K. Kaźmierczak, D. Yi, A. Jaud, P.-F. Fazzini, M. Estrader, G. Viau, P. Decorse, J.-Y. Piquemal, C. Michel, M. Besson, K. Soulantica and N. Perret, Influence of Capping Ligands on the Catalytic Performances of Cobalt Nanoparticles Prepared with the Organometallic Route, *J. Phys. Chem. C*, 2021, **125**, 7711–7720.
35 K. R. Kahsar, D. K. Schwartz and J. W. Medlin, Control of Metal Catalyst Selectivity through Specific Noncovalent Molecular Interactions, *J. Am. Chem. Soc.*, 2014, **136**, 520–526.
36 C. Michel, F. Auneau, F. Delbecq and P. Sautet, C–H versus O–H Bond Dissociation for Alcohols on a Rh(111) Surface: A Strong Assistance from Hydrogen Bonded Neighbors, *ACS Catal.*, 2011, **1**, 1430–1440.
37 C. Michel, F. Göltl and P. Sautet, Early stages of water/hydroxyl phase generation at transition metal surfaces – synergetic adsorption and O–H bond dissociation assistance, *Phys. Chem. Chem. Phys.*, 2012, **14**, 15286.
38 M. Garcia-Ratés, R. García-Muelas and N. López, Solvation Effects on Methanol Decomposition on Pd(111), Pt(111), and Ru(0001), *J. Phys. Chem. C*, 2017, **121**, 13803–13809.

39 S. Wang, V. Vorotnikov and D. G. Vlachos, Coverage-Induced Conformational Effects on Activity and Selectivity: Hydrogenation and Decarbonylation of Furfural on Pd(111), *ACS Catal.*, 2015, **5**, 104–112.
40 H. Hu, A. Ramzan, R. Wischert, F. Jerôme, C. Michel, K. de Olivera Vigier and M. Pera-Titus, Pivotal role of H 2 in the isomerisation of isosorbide over a Ru/C catalyst, *Catal. Sci. Technol.*, 2021, **11**, 7973–7981.
41 P. Pandey, I. Dutta and J. K. Bera, Acceptorless Alcohol Dehydrogenation: A Mechanistic Perspective, *Proc. Natl. Acad. Sci., India, Sect. A*, 2016, **86**, 561–579.
42 X. Wu, S. N. Steinmann and C. Michel, Gaussian attractive potential for carboxylate/cobalt surface interactions, *J. Chem. Phys.*, 2023, **159**, 164115.
43 G. Kresse and J. Hafner, *Phys. Rev. B.*, 1993, **47**, 558–561.
44 J. P. Perdew, K. Burke and M. Ernzerhof, Generalized Gradient Approximation Made Simple, *Phys. Rev. Lett.*, 1996, **77**, 3865–3868.
45 S. N. Steinmann and C. Corminboeuf, Comprehensive benchmarking of a density-dependent dispersion correction, *J. Chem. Theory Comput.*, 2011, **7**, 3567–3577.
46 S. N. Steinmann and C. Corminboeuf, A generalized-gradient approximation exchange hole model for dispersion coefficients, *J. Chem. Phys.*, 2011, **134**, 044117.
47 G. Kresse and D. Joubert, From ultrasoft pseudopotentials to the projector augmented-wave method, *Phys. Rev. B: Condens. Matter Mater. Phys.*, 1999, **59**, 1758–1775.
48 P. E. Blochl, Projector augmented–+rave method, *Phys. Rev. B: Condens. Matter Mater. Phys.*, 1994, **50**, 17953–17979.
49 H. J. Monkhorst and J. D. Pack, Special points for Brillonin-zone integrations, *Phys. Rev. B*, 1976, **13**, 5188–5192.
50 D. Sheppard, R. Terrell and G. Henkelman, Optimization methods for finding minimum energy paths, *J. Chem. Phys.*, 2008, **128**, 134106.
51 G. Henkelman, B. P. Uberuaga and H. Jónsson, A climbing image nudged elastic band method for finding saddle points and minimum energy paths, *J. Chem. Phys.*, 2000, **113**, 9901–9904.
52 J. Kästner and P. Sherwood, Superlinearly converging dimer method for transition state search, *J. Chem. Phys.*, 2008, **128**, 014106.
53 G. Henkelman and H. Jónsson, A dimer method for finding saddle points on high dimensional potential surfaces using only first derivatives, *J. Chem. Phys.*, 1999, **111**, 7010–7022.
54 S. Kozuch and S. Shaik, *Acc. Chem. Res.*, 2011, **44**, 101–110.
55 J. E. Sutton and D. G. Vlachos, Ethanol Activation on Closed-Packed Surfaces, *Ind. Eng. Chem. Res.*, 2015, **54**, 4213–4225.
56 W. Luo and A. Asthagiri, Density Functional Theory Study of Methanol Steam Reforming on Co(0001) and Co(111) Surfaces, *J. Phys. Chem. C*, 2014, **118**, 15274–15285.
57 J. Zaffran, C. Michel, F. Delbecq and P. Sautet, Towards more accurate prediction of activation energies for polyalcohol dehydrogenation on transition metal catalysts in water, *Catal. Sci. Technol.*, 2016, **6**, 6615–6624.
58 K. Kaźmierczak, P. Clabaut, R. Staub, N. Perret, S. N. Steinmann and C. Michel, Designing Active Sites for Structure-Sensitive Reactions via the Generalized Coordination Number: Application to Alcohol Dehydrogenation, *J. Phys. Chem. C*, 2021, **125**, 10370–10377.

